Nanoscale Res Lett (2008) 3:530–533
DOI 10.1007/s11671-008-9194-5

NANO EXPRESS

Structural Evolution During Formation and Filling of Self-patterned Nanoholes on GaAs (100) Surfaces

K. A. Sablon · Zh. M. Wang · G. J. Salamo · Lin Zhou · David J. Smith

Received: 13 October 2008 / Accepted: 17 October 2008 / Published online: 4 November 2008

Abstract Nanohole formation on an AlAs/GaAs superlattice gives insight to both the "drilling" effect of Ga droplets on AlAs as compared to GaAs and the hole-filling process. The shape and depth of the nanoholes formed on GaAs (100) substrates has been studied by the cross-section transmission electron microscopy. The Ga droplets "drill" through the AlAs layer at a much slower rate than through GaAs due to differences in activation energy. Refill of the nanohole results in elongated GaAs mounds along the [01−1] direction. As a result of capillarity-induced diffusion, GaAs favors growth inside the nanoholes, which provides the possibility to fabricate GaAs and AlAs nanostructures.

Keywords Atomic force microscopy · Transmission electron microscopy · Molecular beam epitaxy

Over the past decade, there has been much emphasis directed toward semiconductor nanostructures [1–4]. One area of epitaxial growth that has attracted attention is that of droplet epitaxy for lattice-matched systems [5, 6]. High-temperature droplet epitaxy is a versatile technique: with the right growth conditions, an intriguing range of nanostructures such as nanoholes, double ring-like structures, and quantum dot (QD) molecules can be obtained [7–12]. Among the many nanostructures fabricated by this method, one interesting structure is the nanohole formed on GaAs (100) substrates.

Many types of *top-down* patterning processes have been investigated as an alternative approach to utilizing strain fields as the driving force for growing strained QDs as occurs in the Stranski-Krastanow (SK) growth method [13, 14]. Thus, a range of processes, including electron-beam lithography (EBL), X-ray lithography, extreme-ultraviolet (EUV) lithography, and nanoelectrode lithography [15–18], have been employed for developing surface templates in an effort to obtain lateral patterning of nanostructures. Consequently, the patterned nanostructures are limited in size by lithographic features as well as the presence of defects that result from these processes [18]. The self-limiting inverted-pyramid templating approach proposed by Biasiol and co-authors [19] requires an additional ex situ processing step, but it results in better nanostructure uniformity, since it overcomes the intrinsic randomness of the nucleation process while maintaining high crystal quality at the interface.

The approach described in this article relates to the self-patterning process on GaAs (100) using Ga nanodrills [7]. One of the merits of this in situ approach is that defect-free structures can be realized. The self-patterned GaAs (100) surface has been recently used to initiate the growth of QD clusters as well as low-density QD arrays [20, 21]. In order to better understand the formation of nanoholes and the way in which they are refilled, superlattices of AlAs/GaAs were grown. Two different cases are presented: (1) growth of the superlattice on GaAs (100) followed by nanohole formation, as shown in Fig. 1a, and (2) nanohole formation on GaAs (100) followed by the growth of the superlattice, as shown in Fig. 1b. The most notable features are the refill

K. A. Sablon (✉) · Zh. M. Wang · G. J. Salamo
Institute of Nanoscale Science and Engineering,
University of Arkansas, Fayetteville, AR 72701, USA
e-mail: ksablon@uark.edu

L. Zhou · D. J. Smith
Department of Physics, Arizona State University, Tempe,
AZ 85287, USA

of the top AlAs/GaAs material and the hole formation in the AlAs region of the superlattice.

For this investigation, all samples were grown on semi-insulating GaAs (100) substrates by molecular beam epitaxy (MBE) in a Riber 32. Following oxide desorption and growth of a 0.5 μm GaAs buffer layer at 600 °C, the substrate was cooled down to 500 °C. Sample A was grown by depositing 20 periods (6/6 nm) of AlAs/GaAs, followed by 20 monolayers of Ga droplets, with a growth interruption (GI) and the arsenic valve fully closed for 1 min and 20 s. The sample was then annealed with exposure to the Ga droplets under As flux 1.0×10^{-6} Torr for 100 s before deposition of the AlAs/GaAs superlattice. The growth for sample B was performed in the reverse sequence to that of sample A.

The samples were removed from the MBE system and analyzed using atomic force microscopy (AFM) and transmission electron microscopy (TEM). The specimens were prepared for electron microscope examination in cross-sectional geometry using standard thinning procedures. Cross-section samples were sliced mechanically, polished, dimpled, and then ion-milled to perforation using a 4.0-keV argon ion beam. Bright-field and high-resolution electron micrographs were recorded with a JEOL JEM-4000EX high-resolution electron microscope operated at 400 keV. Cross-section samples were tilted to a [110]-type projection so that the ML planes would be aligned parallel to the incident electron beam direction.

The AFM results of Fig. 1a shows that nanoholes on the AlAs/GaAs superlattices are "square" shaped with an average diameter, $l = 91$ nm and depth, $d = 11.6$ nm with an anisotropic lobe of $h = 10.7$ nm along the [01−1] direction and 8.1 nm along the [011] direction. In contrast, Fig. 1b shows that the surface of sample B consists of GaAs mounds that are greatly elongated along the [01−1] direction, which is attributed to higher diffusion in that direction. The mounds are 4.5 nm in height, 1 μm in the [01−1] direction, and 200 nm in the [011] direction. The depth of the nanohole beneath the superlattice is 15.3 nm and the diameter, $l = 44.8$ nm.

Figure 2a is a cross-sectional electron micrograph of sample B showing the anisotropic nature of the nanohole formed on the GaAs (100) substrate. The raised edges of the nanohole are gradually flattened during growth of the SL. Figure 2a illustrates the refill process of the nanoholes. The disruption from the nanohole slowly disappears as the lattice grows and the surfaces above the nanoholes are higher and not completely flat. This is consistent with the AFM image of Fig. 1b, where GaAs mounds are visible on the surface. This refill of the nanoholes is due to the

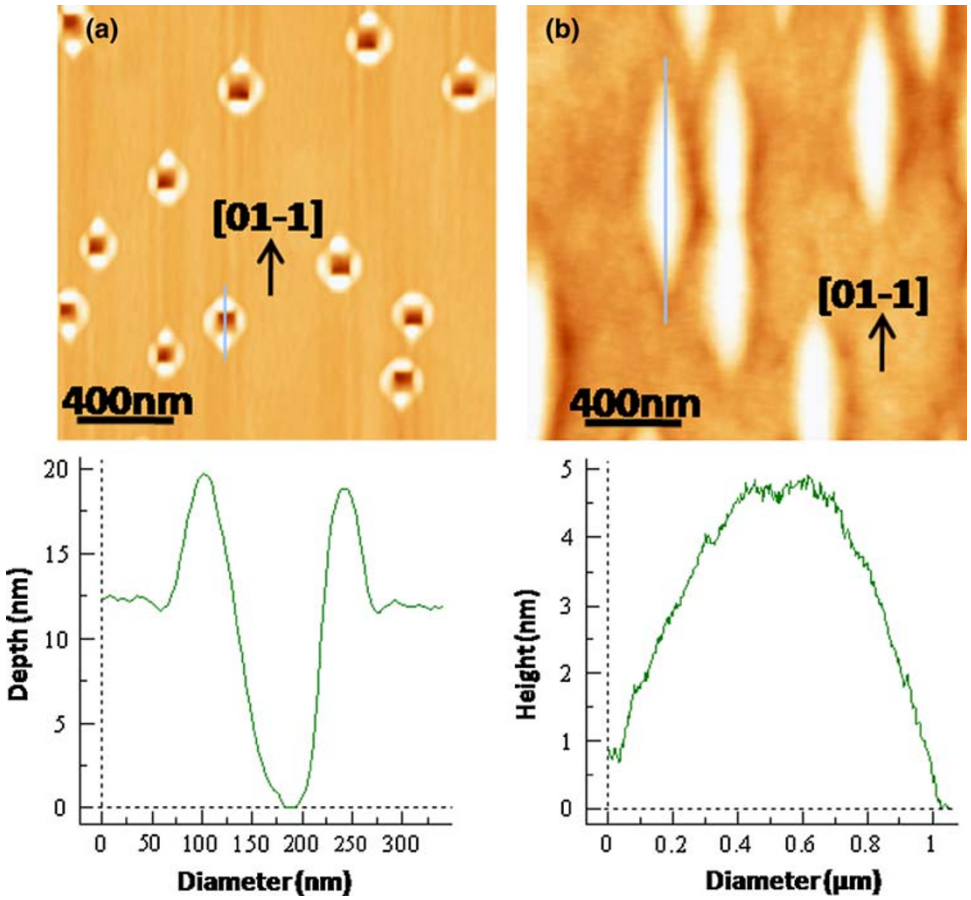

Fig. 1 **a** 2 μm × 2 μm AFM image showing nanoholes on AlAs/GaAs superlattice; **b** 2 μm × 2 μm AFM image of GaAs mounds that result from the re-fill process of nanoholes on GaAs (100)

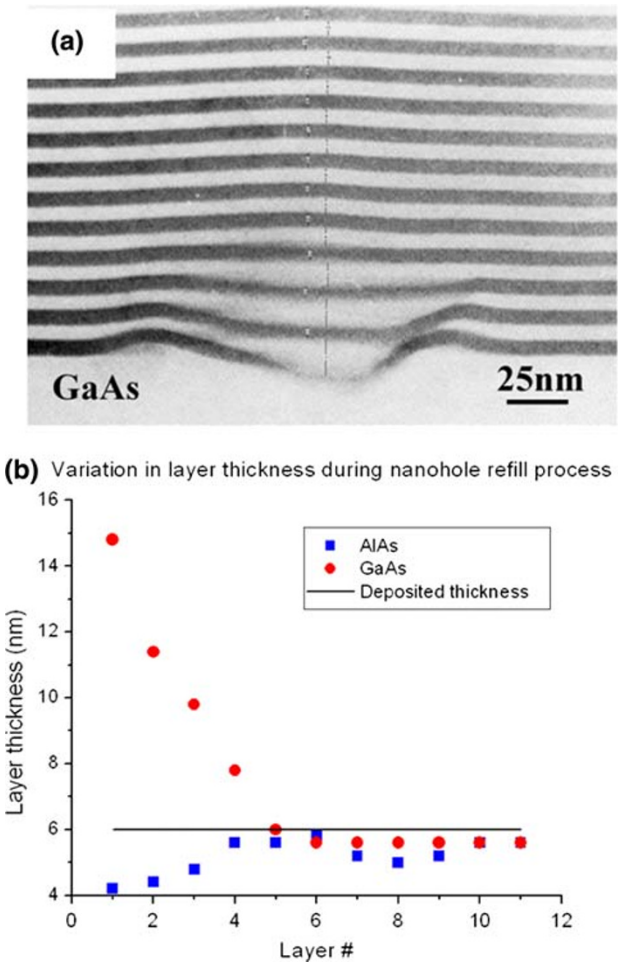

Fig. 2 **a** XTEM micrograph showing the refill process of nanoholes by AlAs/GaAs superlattice. Sample tilted to [110]-type projection; **b** plot that illustrates the refill process

continuous diffusion of GaAs and AlAs atoms from the lobed regions. As this process continues, the holes become refilled layer-by-layer until GaAs mounds are formed on the surface. These mounds assume an elongated shape due to the higher mobility of Ga atoms at high temperatures and higher anisotropy of diffusion in the [01−1] direction on GaAs (100). Note that the central area of the hole appear with a lighter contrast due to the integration of GaAs with AlAs in projection along the electron beam direction. In general, we may expect AlAs to be the same thickness in the center as on the sides. A quantitative view of the refill process is summarized in the graph of Fig. 2b, which illustrates the deposited thickness of 6 nm and the pattern in which the holes are refilled. As the refill process continues, the thickness of GaAs decreases to approach the deposited thickness of 6 nm, while the opposite is true for AlAs. The plot of Fig. 2b illustrates clearly the variation in layer thickness from the deposited thickness of ∼6 nm during the nanohole formation and refill process.

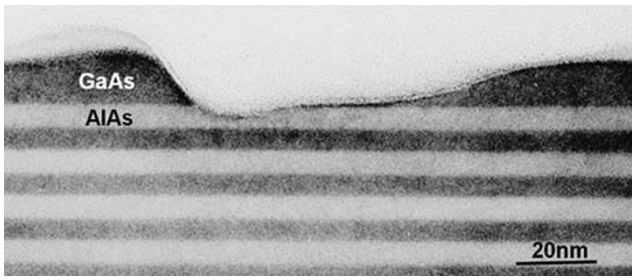

Fig. 3 XTEM micrograph showing nanohole formation on the AlAs/GaAs superlattice. Sample tilted to a [110]-type projection

Figure 3 is an XTEM micrograph of sample A and depicts the nanohole formation through a "layer-by-layer" etch method of the Ga droplets through GaAs and AlAs. The true shape of the nanohole is revealed in this figure. The depth of the hole is 20 nm on average with a diameter of 82 nm. The etched materials have clearly piled up on the edges of the nanohole. We also see a clear separation of AlAs and GaAs, which suggests that GaAs is etched first and subsequently AlAs, which explains the difference in the thicknesses of the respective lobes. The GaAs lobe has a thickness of 13.4 nm, while the AlAs lobe has a thickness of 5.4 nm. Another important feature is that there is no evidence of interdiffusion between the AlAs and GaAs during the etching process. The difference in etching between the AlAs and GaAs is due to the higher activation energy of AlAs, which means that the Ga droplets etch the AlAs layer but at a slower rate. The lattice below the nanohole is uniform. In addition, one side of the nanohole seems abrupt, while the other side is sloping. This shape is consistent with the lobes observed in the AFM image of sample A in Fig. 1a.

In terms of nanohole formation, the u-shaped hole appears to contain thicker material at the bottom compared to the sides, as seen at the bottom of the superlattice in Fig. 2a and atop the superlattice in Fig. 3. This appearance is most likely due to the anisotropy in the growth rates along different crystallographic directions as well as capillarity-induced diffusion of the different underlying materials, with lower diffusion length [22]. In fact, in the absence of capillarity-induced fluxes, growth-rate anisotropy becomes the dominant mechanism, thus suppressing the bottom of the nanohole and yielding high-surface curvature. However, for this case, the growth rate anisotropy does not favor growth on the sidewalls of the self-patterned nonplanar surfaces, and lateral surface fluxes of adatoms are not driven to the bottom of the nanoholes, as reported in Ref. [22]. Further, the expansion in the nanohole width seems to be due to the lower growth rate on the sidewall (see Fig. 3) since growth rate depends on flux in MBE growth [21]. In addition, the self-limiting width of the nanoholes seems to be determined mainly by the arsenic

desorption rate at the interface between the Ga droplets and the GaAs (100) surface, as well as the dependence of capillarity fluxes on the adatom diffusion length as a function of the growth conditions [22].

In summary, we have demonstrated the structural evolution from nanohole formation to GaAs mounds. During the re-fill process, a reasonably uniform superlattice is maintained although the regions of the lattice directly above the holes are higher than the regions in between the holes. During nanohole formation, the bottoms of the holes are wide due to balance between the lower growth rate on the sidewall and the capillarity-induced diffusion. More important, we have demonstrated that Ga droplets do in fact etch AlAs but do so very slowly. Furthermore, as the refill process proceeds, the respective layer thicknesses approach the deposited thickness of 6 nm.

Acknowledgments The authors acknowledge the financial support of the NSF through Grant No. DMR-0520550 and the ONR through Grant No. N00014-00-1-0506. We also acknowledge the use of facilities in the John M. Cowley Center for High-Resolution Electron Micrograph at Arizona State University.

References

1. E. Kapon, Semiconduct. Semimet. **40**, 259 (1994)
2. D. Bouwmeester, A. Ekert, A. Zelinger, *The Physics of Quantum Information Processing* (Springer, Berlin, 2000)
3. A.P. Alivastos, Science **271**, 933 (1996). doi:10.1126/science.271.5251.933
4. Q. Xie, P. Chen, A. Madhukar, Appl. Phys. Lett. **65**, 16 (1994). doi:10.1063/1.113057
5. N. Koguchi, K. Ishige, Jpn. J. Appl. Phys. **32**, 2052 (1993). doi:10.1143/JJAP.32.2052
6. Z.M. Wang, K. Holmes, Y.I. Mazur, K.A. Ramsey, G.J. Salamo, Nanoscale Res. Lett. **1**, 57 (2006). doi:10.1007/s11671-006-9002-z
7. Z.M. Wang, B.L. Liang, K.A. Sablon, G.J. Salamo, Appl. Phys. Lett. **90**, 113120 (2007). doi:10.1063/1.2713745
8. J.H. Lee, Z.M. Wang, Z.Y. Abuwaar, N.W. Strom, G.J. Salamo, Nanotechnology **17**, 3973–3976 (2006). doi:10.1088/0957-4484/17/15/061
9. K.A. Sablon, J.H. Lee, Z.M. Wang, J.H. Shultz, G.J. Salamo, Appl. Phys. Lett. **92**, 20 (2008). doi:10.1063/1.2924308
10. (a) S.-S. Li, J.-B. Xia, Appl. Phys. Lett. **91**, 092119 (2007); (b) S.-S. Li, J.-B. Xia, Nanoscale Res. Lett. **1**, 167 (2006). doi:10.1007/s11671-006-9010-z
11. J.H. Lee, K. Sablon, Z.M. Wang, G.J. Salamo, J. Appl. Phys. **103**, 054301 (2008). doi:10.1063/1.2890149
12. P. Alonso-Gonzalez, B. Alén, D. Fuster, Y. González, L. González, Appl. Phys. Lett. **91**, 163104 (2007)
13. D. Leonard, M. Krishnamurthy, C.M. Reaves, S.P. Denbaars, P.M. Petroff, Appl. Phys. Lett. **63**, 3203 (1993). doi:10.1063/1.110199
14. I.N. Stranski, L. Krastanow, AMA Arch Ophthalmol **146**, 797 (1937)
15. E.S. Snow, P.M. Campbell, P.J. McMarr, Appl. Phys. Lett. **63**, 749 (1993). doi:10.1063/1.109924
16. A. Majumder, P.I. Oden, J.P. Carrejo, L.A. Nagahara, J.J. Graham, J. Alexander, Appl. Phys. Lett. **61**, 2293 (1992). doi:10.1063/1.108268
17. Y. Chen, A.M. Goldman, Appl. Phys. Lett. **91**, 063119 (2007). doi:10.1063/1.2768891
18. Y. Matsuzaki, S. Hasui, S. Kamada, A. Yamada, M. Konagai, Jpn. J. Appl. Phys. **40**, 4325 (2001). doi:10.1143/JJAP.40.4325
19. G. Biasiol, A. Gustafsson, K. Leifer, E. Kapon, Phys. Rev. B **65**, 205306 (2002). doi:10.1103/PhysRevB.65.205306
20. B.L. Liang, Z.M. Wang, J.H. Lee, K. Sablon, Y.I. Mazur, G.J. Salamo, Appl. Phys. Lett. **89**, 043113 (2006). doi:10.1063/1.2244043
21. Zh.M. Wang, B.L. Liang, K. Sablon, J.H. Lee, Y.I. Mazur, N.W. Strom, G.J. Salamo, Small **3**, 2 (2007)
22. E. Kapon, *Pyramidal Quantum Dots Grown on Patterned Substrates* (Springer-Verlag, Berlin, 2007)